Two-dimensional digital image correlation for in-plane displacement and strain measurement: a review

2009 Meas. Sci. Technol. 20 062001

(http://iopscience.iop.org/0957-0233/20/6/062001)

Meas. Sci. Technol. **20** (2009) 062001 (17pp) doi:10.1088/0957-0233/20/6/062001

TOPICAL REVIEW

Two-dimensional digital image correlation for in-plane displacement and strain measurement: a review

Bing Pan[1,4], **Kemao Qian**[2], **Huimin Xie**[3] **and Anand Asundi**[1]

[1] School of Mechanical and Aerospace Engineering, Nanyang Technological University, 639798, Singapore
[2] School of Computing Engineering, Nanyang Technological University, 639798, Singapore
[3] School of Aerospace, FML, Tsinghua University, Beijing 100084, People's Republic of China

E-mail: panb04@mails.tsinghua.edu.cn

Received 14 August 2008, in final form 7 March 2009
Published 27 April 2009
Online at stacks.iop.org/MST/20/062001

Abstract
As a practical and effective tool for quantitative in-plane deformation measurement of a planar object surface, two-dimensional digital image correlation (2D DIC) is now widely accepted and commonly used in the field of experimental mechanics. It directly provides full-field displacements to sub-pixel accuracy and full-field strains by comparing the digital images of a test object surface acquired before and after deformation. In this review, methodologies of the 2D DIC technique for displacement field measurement and strain field estimation are systematically reviewed and discussed. Detailed analyses of the measurement accuracy considering the influences of both experimental conditions and algorithm details are provided. Measures for achieving high accuracy deformation measurement using the 2D DIC technique are also recommended. Since microscale and nanoscale deformation measurement can easily be realized by combining the 2D DIC technique with high-spatial-resolution microscopes, the 2D DIC technique should find more applications in broad areas.

Keywords: digital image correlation, displacement/deformation measurement

(Some figures in this article are in colour only in the electronic version)

1. Introduction

Surface deformation measurement of materials and structures subjected to various loadings (e.g. mechanical loading or thermal loading) is an important task of experimental solid mechanics. Aside from the widely used pointwise strain gauge technique, various full-field non-contact optical methods [1], including both interferometric techniques, such as holography interferometry, speckle interferometry and moiré interferometry, and non-interferometric techniques, such as the grid method [2, 3] and digital image correlation (DIC), have been developed and applied for this purpose. Interferometric metrologies require a coherent light source, and the measurements are normally conducted in a vibration-isolated optical platform in the laboratory. Interferometric techniques measure the deformation by recording the phase difference of the scattered light wave from the test object surface before and after deformation. The measurement results are often presented in the form of fringe patterns; thus, further fringe processing and phase analysis techniques are required. Non-interferometric techniques determine the surface deformation by comparing the gray intensity changes of the object surface before and after deformation, and generally have less stringent requirements under experimental conditions.

[4] Author to whom any correspondence should be addressed.

As a representative non-interferometric optical technique, the DIC method has been widely accepted and commonly used as a powerful and flexible tool for the surface deformation measurement in the field of experimental solid mechanics. It directly provides full-field displacements and strains by comparing the digital images of the specimen surface in the un-deformed (or reference) and deformed states respectively. In principle, DIC is an optical metrology based on digital image processing and numerical computing. It was first developed by a group of researchers at the University of South Carolina in the 1980s [4–9] when digital image processing and numerical computing were still in their infancy [9]. In numerous literature actually the same technique has been given different names, such as digital speckle correlation method (DSCM) [10, 11], texture correlation [12], computer-aided speckle interferometry (CASI) [13, 14] and electronic speckle photography (ESP) [15–18]. Nevertheless, the method is called DIC in this review, considering its popularity in most of the published literature. Besides, it is worth noting that particle image velocity (PIV) [19–21], which has been widely used in experimental fluid mechanics for tracking the velocities of particles seeded in fluids, is very similar to DIC in principle and implementation algorithm. Direct applications of PIV for deformation measurement of soil [22] and metal [23] have also been reported. Interested readers can find more details of PIV in [19–21].

During the past few years, the DIC method has been extensively investigated and significantly improved for reducing computation complexity, achieving high accuracy deformation measurement and expanding application range. For example, the two-dimensional (2D) DIC method using a single fixed camera is limited to in-plane deformation measurement of the planar object surface. To obtain reliable measurements, some requirements on the measuring system must be met [8, 9]. If the test object is of a curved surface, or three-dimensional (3D) deformation occurs after loading, the 2D DIC method is no longer applicable. To overcome this disadvantage of 2D DIC, 3D DIC based on the principle of binocular stereovision [24–27] was developed. Besides, the digital volume correlation (DVC) method, as a direct 3D extension of a 2D DIC method, has also been proposed by Bay and Smith *et al* [28, 29], which provides the internal deformation of solid objects by tracking the movement of volume unit within digital image volumes of the object. The DVC method emerges as a novel and effective tool for measuring the internal deformation of solid objects. However, in this review, we only focus on the 2D DIC method for in-plane displacement and strain measurement.

It should be noted first that both laser speckle patterns [13, 15–17, 30] and artificial white-light speckle patterns (or more accurately, the random gray intensity pattern of the object surface) have been used as the carrier of surface deformation information in 2D DIC. The laser speckle pattern can be produced by illuminating the optically rough surface with a coherent light source (laser beam). However, a serious decorrelation effect occurs in laser speckle patterns when the test object is subjected to rigid body motion, excessive straining as well as out-of-plane displacement [31], which prevents its practicality. In contrast, the white-light speckle 2D DIC is more robust and appealing. Indeed, it can easily be found that most of the current publications with regard to DIC employ white-light speckle patterns, which used a white light source or natural light illumination.

Compared with the interferometric optical techniques used for in-plane deformation measurement, the 2D DIC method has both advantages and disadvantages. For instance, it offers the following special and attractive advantages [8, 9, 32].

(1) *Simple experimental setup and specimen preparation*: only one fixed CCD camera is needed to record the digital images of the test specimen surface before and after deformation. Specimen preparation is unnecessary (if the natural texture of a specimen surface has a random gray intensity distribution) or can simply be made by spraying paints onto the specimen surface.
(2) *Low requirements in measurement environment*: 2D DIC does not require a laser source. A white light source or natural light can be used for illumination during loading. Thus, it is suitable for both laboratory and field applications.
(3) *Wide range of measurement sensitivity and resolution*: Since the 2D DIC method deals with digital images, thus the digital images recorded by various high-spatial-resolution digital image acquisition devices can be directly processed by the 2D DIC method. For example, 2D DIC can be coupled with optical microscopy [33–35], laser scanning confocal microscope (LSCM) [36, 37], scanning electron microscopy (SEM) [38–47], atomic force microscopy (AFM) [48–58] and scanning tunneling microscope (STM) [59–61] to realize microscale to nanoscale deformation measurement. Similarly, the instantaneous deformation measurement can be realized by analyzing the dynamic sequence of digital images recorded with high-speed digital image recording equipment using the 2D DIC method [62–69].

More importantly, with the constant emergence of high-spatial-resolution and high-time-resolution image acquisition equipment, the 2D DIC method can easily be applied to new areas. So, it can be said that the 2D DIC method is one of the current most active optical measurement technologies, and demonstrates increasingly broad application prospects.

Nevertheless, the 2D DIC method also suffers some disadvantages: (1) the test planar object surface must have a random gray intensity distribution; (2) the measurements depend heavily on the quality of the imaging system; (3) at present, the strain measurement accuracy of the 2D DIC method is lower than that of interferometric techniques, and is not recommended as an effective tool for non-homogeneous small deformation measurement.

Although numerous literature regarding 2D DIC can be found, there still lacks a review paper which focuses on the technical details and accuracy analysis of the simple and widely used optical method. A more detailed review of this method therefore seems to be necessary. The purpose of this review is to systematically overview the

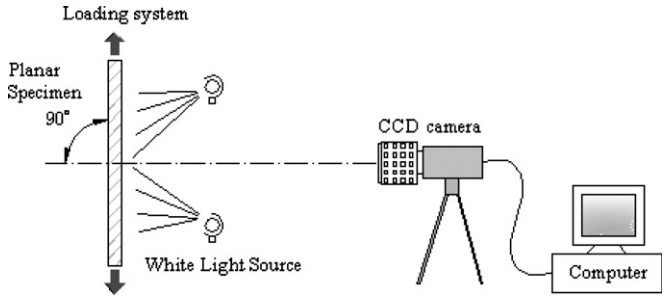

Figure 1. Typical optical image acquisition system for the 2D DIC method.

technical details and advances of the 2D DIC method. Emphasis is placed on the introduction of displacement field measurement and strain field estimation algorithms, as well as the detailed analysis of the measurement accuracy considering the influences of both experimental conditions and algorithm details.

2. Fundamentals of 2D DIC

In general, the implementation of the 2D DIC method comprises the following three consecutive steps, namely (1) specimen and experimental preparations; (2) recording images of the planar specimen surface before and after loading; (3) processing the acquired images using a computer program to obtain the desired displacement and strain information. In this section, issues on specimen preparation and image capture are introduced first. Then, the basic principles and concepts of 2D DIC are described.

2.1. Specimen preparation and image capture

Figure 1 shows the schematic illustration of a typical experimental setup using an optical imaging device for the 2D DIC method. The specimen surface must have a random gray intensity distribution (i.e. the random speckle pattern), which deforms together with the specimen surface as a carrier of deformation information. The speckle pattern can be the natural texture of the specimen surface or artificially made by spraying black and/or white paints, or other techniques. The camera is placed with its optical axis normal to the specimen surface, imaging the planar specimen surface in different loading states onto its sensor plane.

Since the recorded images are the 2D projection of the specimen surface, the estimated motion of each image point multiplying the magnification of the imaging system (in units of mm/pixel) will not accurately equal that of the actual physical point on the specimen surface, unless the following requirements are met.

(1) The specimen surface must be flat and remain in the same plane parallel to the CCD sensor target during loading [8, 9]. This implies that the CCD sensor and the object surface should be parallel, and out-of-plane motion of the specimen during loading should be small enough to be neglected. The out-of-plane motion of the specimen leads to a change in magnification of the recorded images, which further yields additional in-plane displacements. Thus, it should be avoided for accurate displacement estimation. Normally, the out-of-plane motion can be somewhat alleviated by using a telecentric imaging system or placing the camera far from the specimen to approximate a telecentric imaging system [8, 70].

(2) The imaging system should not suffer from geometric distortion. In an actual optical imaging system or other high-resolution imaging system (e.g. SEM, LSCM or AFM), geometric distortion is more or less presented, which impairs the ideal linear correspondence between the physical point and imaged point and produces additional displacements (see figure 2). If the influence of geometric distortion cannot be neglected, corresponding distortion correction techniques [35, 45–47, 55, 71–73] should be used to remove the influence of distortion to provide accurate measurements.

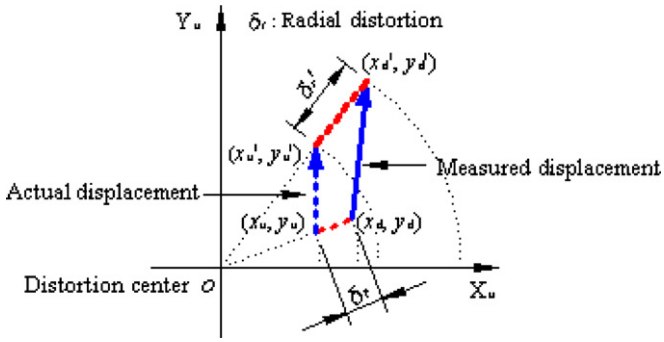

Figure 2. Influence of radial distortion on the measured displacement. (x_u, y_u) and (x_u', y_u') denote the ideal undistorted image coordinates before and after deformation respectively; (x_d, y_d) and (x_d', y_d') denote the actual distorted image coordinates before and after deformation respectively.

2.2. Basic principles and concepts

After recording the digital images of the specimen surface before and after deformation, the DIC computes the motion of each image point by comparing the digital images of the test object surface in different states. In the following, the basic principles and concepts involved in 2D DIC are introduced.

2.2.1. Basic principles. In routine implementation of the 2D DIC method, the calculation area (i.e. region of interest, ROI) in the reference image should be specified or defined at first, which is further divided into evenly spaced virtual grids as shown in figure 3(*a*). The displacements are computed at each point of the virtual grids to obtain the full-field deformation (see figure 3(*b*)).

The basic principle of 2D DIC is the tracking (or matching) of the same points (or pixels) between the two images recorded before and after deformation as schematically illustrated in figure 4. In order to compute the displacements of point P, a square reference subset of $(2M + 1) \times (2M + 1)$ pixels centered at point $P(x_0, y_0)$ from the reference image is chosen and used to track its corresponding location in the deformed image. The reason why a square subset, rather than

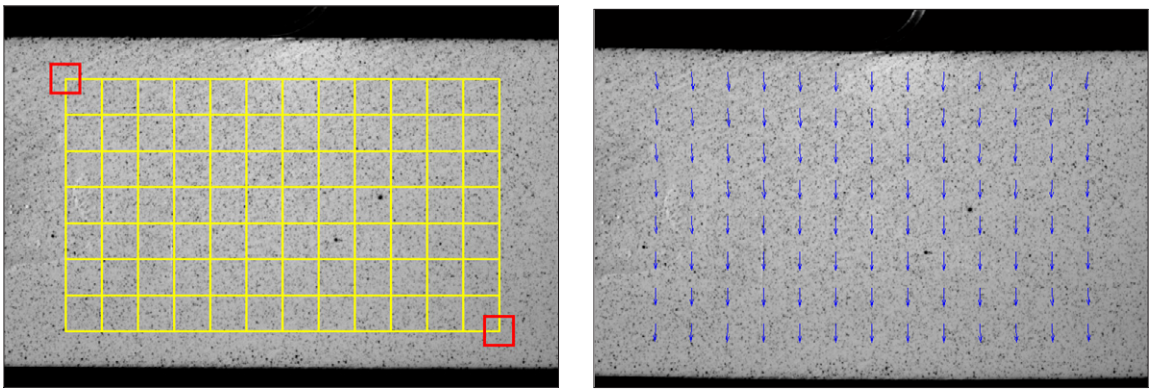

(*a*) (*b*)

Figure 3. (*a*) Reference image, the imposed red square is the subset used for tracking the motion of its center point, and the intersection points of the yellow grid denote the points to be calculated; (*b*) the calculated displacement vectors imposed on the deformed image.

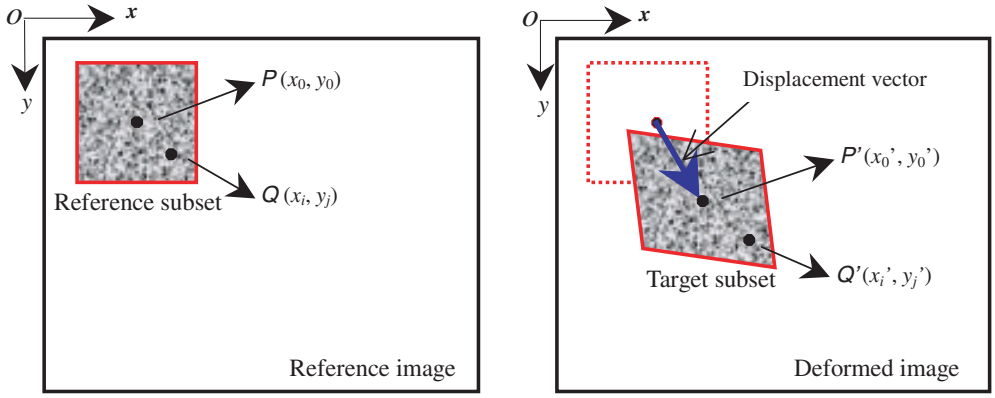

Figure 4. Schematic illustration of a reference square subset before deformation and a target (or deformed) subset after deformation.

an individual pixel, is selected for matching is that the subset comprising a wider variation in gray levels will distinguish itself from other subsets, and can therefore be more uniquely identified in the deformed image.

To evaluate the similarity degree between the reference subset and the deformed subset, a cross-correlation (CC) criterion or sum-squared difference (SSD) correlation criterion must be predefined. The matching procedure is completed through searching the peak position of the distribution of correlation coefficient. Once the correlation coefficient extremum is detected, the position of the deformed subset is determined. The differences in the positions of the reference subset center and the target subset center yield the in-plane displacement vector at point P, as illustrated in figure 4.

2.2.2. Shape function/displacement mapping function. It is reasonable to assume that the shape of the reference square subset is changed in the deformed image. However, based on the assumption of deformation continuity of a deformed solid object, a set of neighboring points in a reference subset remains as neighboring points in the target subset. Thus, as schematically shown in figure 4, the coordinates of point $Q(x_i, y_j)$ around the subset center $P(x_0, y_0)$ in the reference subset can be mapped to point $Q'(x_i', y_j')$ in the target subset according to the so-called shape function [74] or displacement mapping function [75]:

$$\begin{aligned} x_i' &= x_i + \xi(x_i, y_j) \\ y_j' &= y_j + \eta(x_i, y_j) \end{aligned} \qquad (i, j = -M : M). \tag{1}$$

If only rigid body translation exists in the reference subset and deformed subset, in other words, the displacements of each point in the subset are the same, then a zero-order shape function can be used:

$$\xi_0(x_i, y_j) = u \qquad \eta_0(x_i, y_j) = v. \tag{2}$$

Obviously, the zero-order shape function is not sufficient to depict the shape change of the deformed subset. Thus, the first-order shape function that allows translation, rotation, shear, normal strains and their combinations of the subset is most commonly used:

$$\begin{aligned} \xi_1(x_i, y_j) &= u + u_x \Delta x + u_y \Delta y \\ \eta_1(x_i, y_j) &= v + v_x \Delta x + v_y \Delta y. \end{aligned} \tag{3}$$

Besides, the second-order shape functions proposed by Lu *et al* [75] can be used to depict more complicated deformation states of the deformed subset:

$$\xi_2(x_i, y_j) = u + u_x \Delta x + u_y \Delta y + \tfrac{1}{2} u_{xx} \Delta x^2 + \tfrac{1}{2} u_{yy} \Delta y^2 + u_{xy} \Delta x \Delta y$$

Table 1. Commonly used cross-correlation criterion.

CC correlation criterion	Definition
Cross-correlation (CC)	$C_{\mathrm{CC}} = \sum_{i=-M}^{M}\sum_{j=-M}^{M}[f(x_i, y_j)g(x_i', y_j')]$
Normalized cross-correlation (NCC)	$C_{\mathrm{NCC}} = \sum_{i=-M}^{M}\sum_{j=-M}^{M}\left[\frac{f(x_i, y_j)g(x_i', y_j')}{\bar{f}\bar{g}}\right]$
Zero-normalized cross-correlation (ZNCC)	$C_{\mathrm{ZNCC}} = \sum_{i=-M}^{M}\sum_{j=-M}^{M}\left\{\frac{[f(x_i, y_j) - f_m] \times [g(x_i', y_j') - g_m]}{\Delta f \Delta g}\right\}$

Table 2. Commonly used SSD correlation criterion.

SSD correlation criterion	Definition
Sum of squared differences (SSD)	$C_{\mathrm{SSD}} = \sum_{i=-M}^{M}\sum_{j=-M}^{M}[f(x_i, y_j) - g(x_i', y_j')]^2$
Normalized sum of squared differences (NSSD)	$C_{\mathrm{NSSD}} = \sum_{i=-M}^{M}\sum_{j=-M}^{M}\left[\frac{f(x_i, y_j)}{\bar{f}} - \frac{g(x_i', y_j')}{\bar{g}}\right]^2$
Zero-normalized sum of squared differences (ZNSSD)	$C_{\mathrm{ZNSSD}} = \sum_{i=-M}^{M}\sum_{j=-M}^{M}\left[\frac{f(x_i, y_j) - f_m}{\Delta f} - \frac{g(x_i', y_j') - g_m}{\Delta g}\right]^2$

$$\eta_2(x_i, y_j) = v + v_x\Delta x + v_y\Delta y + \tfrac{1}{2}v_{xx}\Delta x^2 + \tfrac{1}{2}v_{yy}\Delta y^2 + v_{xy}\Delta x\Delta y. \quad (4)$$

In equations (2)–(4), $\Delta x = x_i - x_0$, $\Delta y = y_j - y_0$, u, v are the x- and y-directional displacement components of the reference subset center, $P(x_0, y_0)$, u_x, u_y, v_x, v_y are the first-order displacement gradients of the reference subset and $u_{xx}, u_{xy}, u_{yy}, v_{xx}, v_{xy}, v_{yy}$ are the second-order displacement gradients of the reference subset.

2.2.3. Correlation criterion. As already mentioned, to evaluate the similarity degree between the reference and deformed subsets, a correlation criterion should be defined in advance before correlation analysis. Although different definitions of correlation criteria can be found in the literature, these correlation criteria can be categorized into two groups, namely CC criteria and SSD correlation criteria [76, 77] as listed in tables 1 and 2, respectively.

In tables 1 and 2,

$$f_m = \frac{1}{(2M+1)^2}\sum_{i=-M}^{M}\sum_{j=-M}^{M} f(x_i, y_j),$$

$$g_m = \frac{1}{(2M+1)^2}\sum_{i=-M}^{M}\sum_{j=-M}^{M} g(x_i', y_j'),$$

$$\bar{f} = \sqrt{\sum_{i=-M}^{M}\sum_{j=-M}^{M}[f(x_i, y_j)]^2},$$

$$\bar{g} = \sqrt{\sum_{i=-M}^{M}\sum_{j=-M}^{M}[g(x_i', y_j')]^2},$$

$$\Delta f = \sqrt{\sum_{i=-M}^{M}\sum_{j=-M}^{M}[f(x_i, y_j) - f_m]^2},$$

$$\Delta g = \sqrt{\sum_{i=-M}^{M}\sum_{j=-M}^{M}[g(x_i', y_j') - g_m]^2}.$$

It is worth noting that the CC criteria are actually related to the SSD criteria. For example, the ZNCC criterion can be deduced from the ZNSSD correlation criterion, the detailed derivation can be found in [78] and the following relationship can easily be derived as $C_{\mathrm{ZNSSD}}(\mathbf{p}) = 2[1 - C_{\mathrm{ZNCC}}(\mathbf{p})]$. Similarly, the NSSD criterion can also be deduced from the NSSD correlation criterion as $C_{\mathrm{NSSD}}(\mathbf{p}) = 2[1 - C_{\mathrm{NCC}}(\mathbf{p})]$. Also, we should note that if a linear transformation of the target subset gray intensity is made according to the function $g'(x', y') = a \times g(x', y') + b$ [78], the correlation values computed using the ZNCC or ZNSSD correlation criterion remain unchanged. So, it is concluded that the ZNCC or ZNSSD correlation criterion offers the most robust noise-proof performance and is insensitive to the offset and linear scale in illumination lighting. Similarly, the NCC or NSSD correlation criterion is insensitive to the linear scale in illumination lighting but sensitive to offset of the lighting. The CC or SSD correlation criterion is sensitive to all lighting fluctuations.

2.2.4. Interpolation scheme. As can be seen from equation (1), the coordinates of point (x_i', y_j') in the deformed subset may locate between pixels (i.e. sub-pixel location). Before evaluating the similarity between reference and deformed subsets using the correlation criterion defined in tables 1 and 2, the intensity of these points with sub-pixel locations must be provided. Thus, a certain sub-pixel interpolation scheme should be utilized. In the

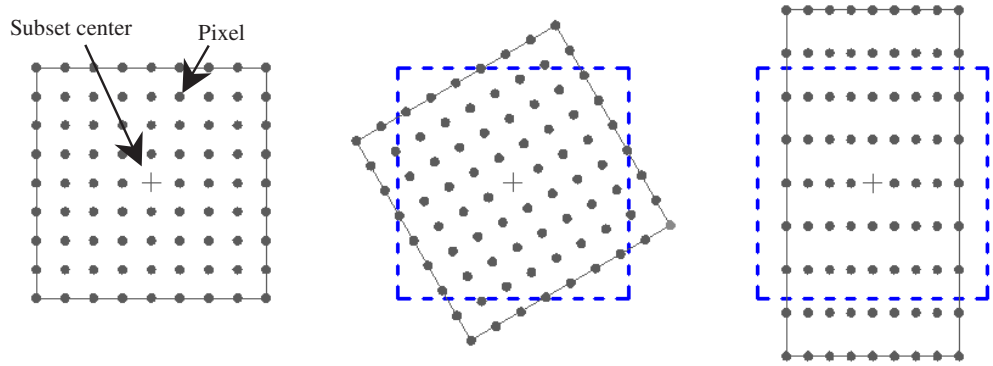

Figure 5. Schematic drawing of a reference subset (left), a subset after rigid body rotation (middle) and a subset after large deformation (right).

literature, various sub-pixel interpolation schemes including bilinear interpolation, bicubic interpolation, bicubic B-spline interpolation, biquintic B-spline interpolation and bicubic spline interpolation have been used. The detailed algorithms of these interpolation schemes can be found in numerical computing books [79]. However, a high-order interpolation scheme (e.g. bicubic spline interpolation or biquintic spline interpolation) is highly recommended by Schreier *et al* [80] and Knauss *et al* [49] since they provide higher registration accuracy and better convergence character of the algorithm than the simple interpolation schemes do.

3. Displacement field measurement

Due to the discrete nature of the digital image, the integer displacements with 1 pixel accuracy can readily be computed. To further improve displacement measurement accuracy, certain sub-pixel registration algorithms should be used [81]. Generally, to achieve sub-pixel accuracy, the implementation of 2D DIC comprises two consecutive steps, namely initial deformation estimation and sub-pixel displacement measurement. In other words, the 2D DIC method normally requires an accurate initial guess of the deformation before achieving sub-pixel accuracy. For example, for the most commonly used iterative spatial cross-correlation algorithm (e.g. the Newton–Raphson method), it only converges when an accurate initial guess is provided (the radius of convergence is estimated to be smaller than 7 pixels in the evaluation tests performed by Vendroux and Knauss [60]). As for the coarse–fine algorithm and the peak-finding algorithm, an integer displacement of 1 pixel resolution must be provided before further sub-pixel displacement registration. For this reason, the techniques for an initial guess of deformation are described first in this section.

3.1. Initial guess of deformation and calculation path

3.1.1. Initial guess of deformation. Usually, the relative deformation or rotation between the reference subset and the deformed subset is quite small, so it is easy to get accurate estimation of the initial displacements by a simple searching scheme implemented either in spatial domain or in frequency domain. In spatial domain, the accurate locations of the target subset can be determined by a fine search routine, pixel by pixel, performed within the specified range in the deformed image. Some schemes, such as the coarse-to-fine and the nested searching schemes [82], can be used to speed up the calculation. These search schemes yield 1 pixel resolution. Alternatively, the correlation between the reference subset and the deformed subset can also be implemented in Fourier domain as conducted and advocated by Chen *et al* [13], Sojahal *et al* [15] and Hild *et al* [83]. In Fourier domain, the correlation between two subsets is calculated as the complex multiplication of the first subset's Fourier spectrum by the complex conjugate of the second subset's spectrum. Since the FFT can be implemented with very high speed, the Fourier domain correlation method is also extremely fast. However, the in-plane translation is implicitly assumed in the Fourier domain method, small strains and/or rotations occuring between the two subsets will lead to significant errors.

The above-mentioned technique performs well for most cases. Difficulties occur in certain cases when large rotation and/or large deformation presents between the reference and target subsets, as schematically shown in figure 5 [84], in which some pixels of the reference subset run out of the area of the assumed subset within the deformed image; consequently, the similarity between the reference subset and the assumed deformed subset will decrease substantially. As can be seen from figure 6(*a*), if only rigid body translation exists between the reference and deformed subsets, a single peak can be found in the correlation coefficient distribution. In contrast, while a 20° relative rotation occurs between the reference image and the deformed image, there will not be even a single sharp peak in the correlation distribution map as indicated in figure 6(*b*), and thus result in a failure in integer pixel displacement searching.

Other techniques are therefore required to achieve a reliable initial guess of deformation in these cases. Inspired by the nested coarse–fine algorithm presented by Zhang *et al* [82] that can provide an initial guess for each calculation point, a technique was presented by Pan *et al* [84] to achieve a reliable initial guess for the NR method for these cases. Slightly different from Zhang's work, this technique only provides the initial guess of the first calculation point. Then, based on the assumption of continuous deformation of solid

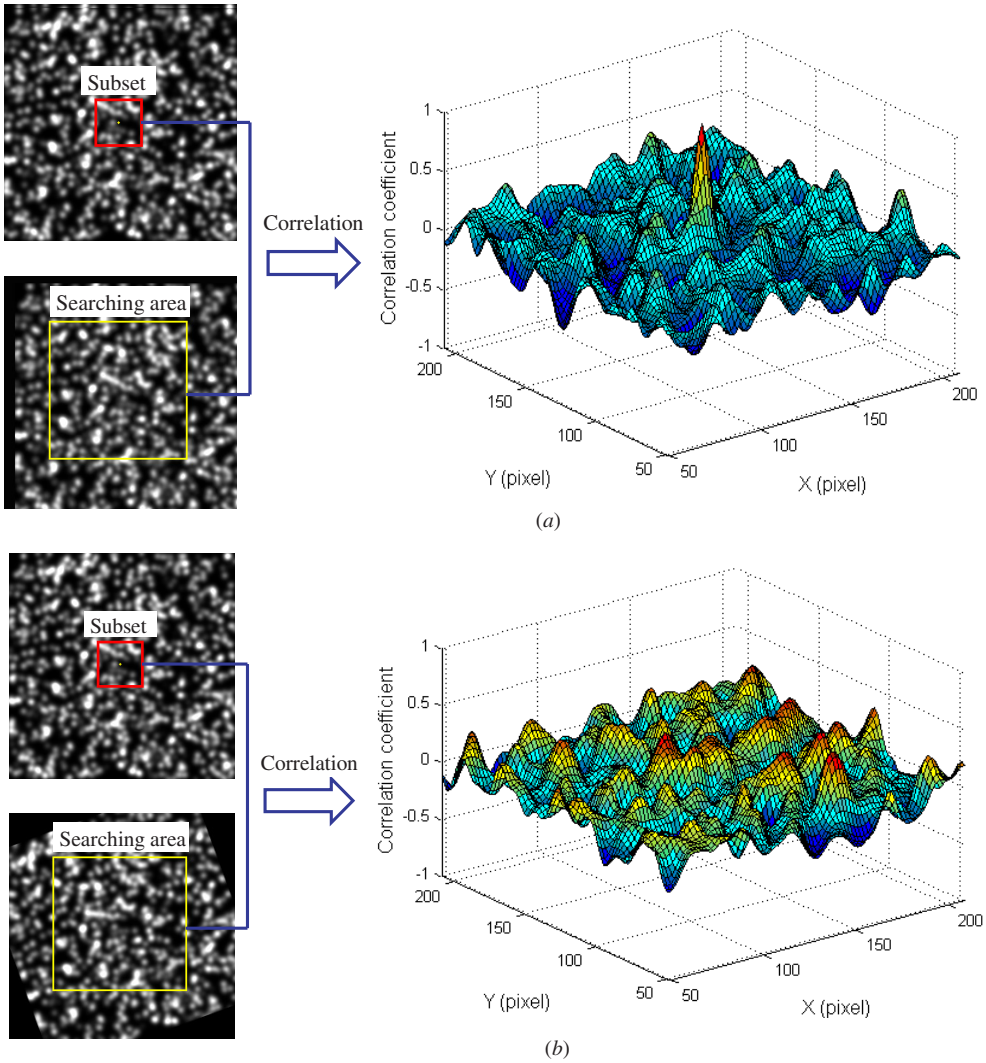

Figure 6. Computed whole-field cross-correlation coefficient distribution when the deformed image is subjected to (*a*) rigid body translation, and (*b*) 20° relative rotation.

object, the obtained result of the first point serves as the initial guess for the next point to be calculated. The initial guess of deformation is determined by manually selecting three or more points (x_i, y_i) $(i = 1, 2, \ldots, n,$ and $n \geqslant 3)$ with distinct features around the reference subset center, and their corresponding locations (x_i', y_j') $(i = 1, 2, \ldots, n,$ and $n \geqslant 3)$ in the deformed image. Thus, the desired initial guess can be resolved from the coordinate correspondence (depicted by the first-order shape function) using the least-squares method. Alternatively, benefiting from the extraordinary ability of its global optimum, the genetic algorithm [85] can also be used as an automatic technique for determining the initial guess of the first calculation point. However, the genetic algorithm normally costs a lot of computation time to converge to the global extremum.

3.1.2. Calculation path. As described in subsection 2.2.1, before the implementation of DIC analysis, ROI should be specified or defined in the reference image. The regularly spaced points within ROI are considered as points to be computed. Conventional correlation calculation generally starts with the upper-left point of the ROI. Then, the calculation analysis is carried out point by point along each row or column. Normally, to speed calculation and save computation time, the computed displacements and strains of the current point are used as the initial guess of the next point according to the continuous deformation assumption. In this sense, the conventional DIC computation is a path-dependent approach. Although we can estimate the initial guess separately for each point, however, this approach is either impractical because it is extremely time-consuming or impossible if large deformation and/or rotation presents in the deformed image. So, even though the well-established conventional DIC method is effective in most cases, this path-dependent approach may give rise to wrong results in the following cases. First, if the digital images of a practical test object contain discontinuous areas such as cracks, holes or other discontinuous area or if an irregular ROI is defined in the reference image, the transfer of the initial guess will fail to provide a reliable initial guess for the next point at some locations. Second, if apparent discontinuous deformation occurs in the deformed image, the

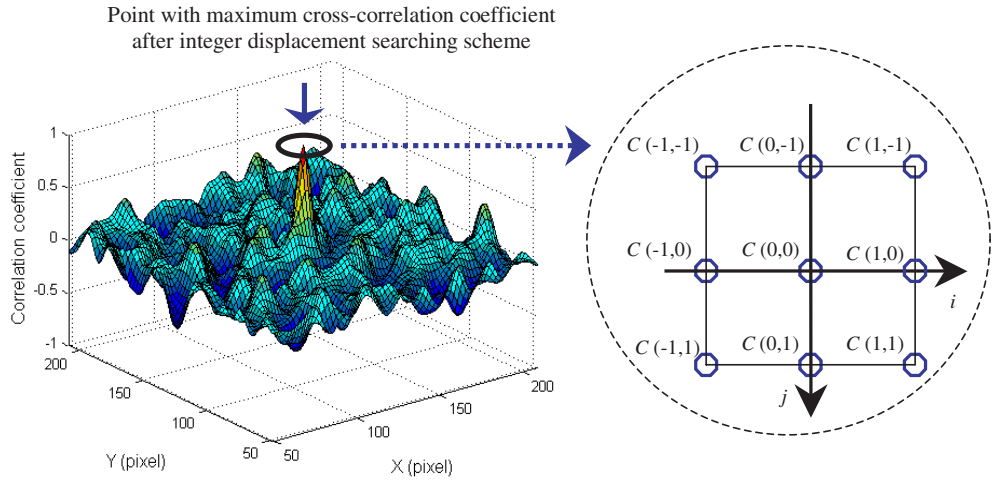

Figure 7. Schematic figure of local discrete correlation coefficient distribution of 3 × 3 points, and $C(0,0)$ is the point with the maximum correlation coefficient obtained from a integer pixel displacement searching scheme.

transfer of the initial guess also fails. Third, occasionally occurring wrong data points will also provide a wrong initial guess for the next point. In all these cases, if one point is wrongly computed, the results of wrong points will be passed to the next point, which leads to the propagation of error.

More recently, a universally applicable reliability-guided DIC (RG-DIC) method has been proposed by Pan [86] for reliable image deformation measurement. In the method, the ZNCC coefficient is used to identify the reliability of the point computed. The correlation calculation begins with a seed point and is then guided by the ZNCC coefficient. That means the neighbors of the point with the highest ZNCC coefficient in a queue for the computed points will be processed first. Thus, the calculation path is always along the most reliable direction and possible error propagation of the conventional DIC method can be entirely avoided. The RG-DIC method is very robust and effective. It is universally applicable to the deformation measurement of images with area and/or deformation discontinuities.

3.2. Sub-pixel displacement registration algorithms

The techniques described above only provide displacements with pixel level accuracy or approximated initial guess of the deformation vector. To further improve the accuracy of DIC, a certain kind of sub-pixel registration algorithm should be used. In the following, various sub-pixel registration algorithms proposed in the literature are introduced and discussed.

3.2.1. Coarse–fine search algorithm. In the determination of integer-pixel displacement, the search method searches the specified searching area of interest with 1 pixel step to find the point with maximum cross-correlation coefficient. It is straightforward to change the search step into 0.1 pixels or 0.01 pixels to achieve a sub-pixel accuracy of 0.1 pixels or 0.01 pixels, respectively [4, 65]. Usually the zero-order shape function is implicitly used in the coarse–fine searching algorithm while implementing the direct searching scheme. The gray level at sub-pixel locations must be reconstructed in advance using certain interpolation scheme, which generally costs long computation time. Some work [82] has been done to reduce the computation cost and the probability of mis-identification of the traditional coarse–fine search algorithm. Nevertheless, compared with the next two algorithms, the coarse–fine method is still time-consuming.

3.2.2. Peak-finding algorithm. The peak-finding algorithm refers to a class of algorithms for detecting the peak position of the local discrete correlation coefficient matrix (typically, 3 × 3 or 5 × 5 pixels) around the pixel with maximum CC coefficient or minimum SSD coefficient after the integer-pixel displacement searching scheme as shown in figure 7. Both least-squares fitting and interpolation algorithms can be used to approximate the local correlation coefficient matrix, and the peak position of the approximated curve surface is taken as the sub-pixel displacements. For example, Chen *et al* [13] proposed a biparabolic least-squares fitting of the local peak and define the peak position to be the extremum of the obtained polynomial; Sjodahl *et al* [15] used the algorithm by expanding the discrete correlation function in terms of a Fourier series first, followed by a numerical searching scheme to find the exact peak; Hung *et al* [87] and other researchers [88–93] employed a two-dimensional quadratic surface fitting of the peak and the sub-pixel displacements are defined based on the location of the maximum value of the fitting surface; and more recently, Wim *et al* [94] computed the sub-pixel displacements by simply calculating the center of mass localization of the discrete correlation matrix. The principle and implementation of peak-finding techniques for sub-pixel displacement measurement is simple, it can be done very fast. However, the peak-finding algorithms do not consider the shape change of the deformed subset, and just compute the approximated peak rather than the actual peak of correlation coefficient; as a consequence, the accuracy is lessened [81, 87].

3.2.3. Iterative spatial domain cross-correlation algorithm. If we take the relative deformation (i.e. shape change) between

the reference and target subsets into account, the correlation function thus becomes a nonlinear function with respect to the desired mapping parameters vector. For example, if the first-order shape function is used, the desired mapping parameters vector is $\mathbf{p} = (u, u_x, u_y, v, v_x, v_y)^T$. To optimize the nonlinear correlation function, a two-parameter iterative algorithm was first developed by Sutton *et al* [95]. However, as pointed out in the same paper, the two-parameter iterative algorithm normally does not converge to the exact solutions unless the correlation function is linear with the desired parameters. Naturally, it has been replaced by the more efficient and accurate Newton–Raphson (NR) algorithm.

As a classic algorithm in 2D DIC, the NR method was also originally presented by Bruck *et al* [95] and was significantly improved by Vendroux and Knuass [60] with an adoption of the approximated Hessian matrix. To get the desired deformation vector, using the NR iteration method, the solution can be written as

$$\mathbf{p} = \mathbf{p}_0 - \frac{\nabla C(\mathbf{p}_0)}{\nabla\nabla C(\mathbf{p}_0)}, \tag{5}$$

where $\mathbf{p}_0$ is the initial guess of the solution, which can be provided by the scheme described in the previous section; $\mathbf{p}$ is the next iterative approximation solution; $\nabla C(\mathbf{p}_0)$ is the gradients of correlation criteria and $\nabla\nabla C(\mathbf{p}_0)$ is the second-order derivation of correlation criteria, commonly called the Hessian matrix. According to the approach proposed by Vendroux and Knauss [60], an approximation can be made to the Hessian matrix that can significantly simplify the calculation process of equation (5) without affecting the calculation accuracy. Except for the improved NR algorithm, the Levenberg–Marquart algorithm (LM) [74] and the quasi-NR [96] were also proposed by some researchers to overcome the shortcoming of the NR algorithm to speed the calculation. Apparently, the iterative spatial domain cross-correlation algorithm is unaffected by large strains and/or rotations of the deformed image, because it is able to take the deformation of a subset into consideration.

3.2.4. Spatial-gradient-based algorithm. Based on the optical flow developed by Davis *et al* [97], an iterative, spatial-gradient-based algorithm was proposed by Zhou *et al* [11] for sub-pixel displacement estimation. The algorithm was further investigated and improved by Zhang *et al* [98], Pan *et al* [99–101] and Meng *et al* [102]. More recently, a generalized spatial-gradient-based DIC method has been developed by Pan *et al* [101] to overcome the limitations of the previous algorithms by taking the scale and offset of the intensity into consideration. In the generalized spatial-gradient-based algorithm, the basic optical flow equation for point (x_i, y_i) within the subset is written as

$$a \times f(x_i, y_j) + b = g(x_i + u + u_x\Delta x_i + u_y\Delta y_i, \\ y + v + v_x\Delta x_i + v_y\Delta y_i) \qquad (i, j = -M : M) \tag{6}$$

where a is the scale factor of the intensity change and b denotes the offset of the intensity change.

Both conventional least-squares and iterative least-squares [101] can then be used to solve the unknown parameter vector, which contains deformation parameters of the subset, the scale factor and the offset of the intensity change. Calculation using least-squares is exempted from sub-pixel interpolation and iteration; thus, it can be implemented with very fast computation speed. However, an iterative least-squares algorithm providing higher accuracy in the computed displacements and displacement gradients is highly recommended. Because only the first-order spatial derivatives (i.e. g_x, g_y) of the deformed image are required during calculation, thus, it is little simpler than the classic NR method. However, the spatial-gradient-based method is actually equivalent to the optimization of the following SSD correlation criterion using an improved NR algorithm as proved by Pan *et al* [101]:

$$C_{\mathrm{SSD}}(\mathbf{p}) = \sum_{i=-M}^{M}\sum_{j=-M}^{M}[g(x_i + u(x_i, y_j), y_j + v(x_i, y_j)) \\ - a \times f(x_i, y_j) - b]^2, \tag{7}$$

where $\mathbf{p}$ denotes the desired parameter vector.

3.2.5. Genetic algorithms. As a random search algorithm with robust global converge capability, the genetic algorithm is widely used to optimize the multi-dimensional nonlinear function, and it was also introduced into the 2D DIC method to optimize the correlation criterion for determination of deformation parameters [84, 103–108]. To detect a global optimum deformation vector for the objective function (i.e. correlation criterion), an initial population containing N candidate individuals (i.e. deformation parameter vector) is randomly generated within its possible range, and then the objective function cost function is evaluated for all the candidate individuals. The best individuals are kept and the worst discarded, and some new individuals are also randomly generated to replenish the population. Subsequently, some schemes, such as crossover, mutation and recombination, are used to generate a new population from the last population and the objective function is evaluated again for all the candidate individuals. These processes are repeated until the converging conditions are satisfied. Although with extraordinary ability of global optimum, the genetic DIC method generally requires a long computation cost to find the global extremum of the correlation coefficient.

3.2.6. Finite element method and B-spline algorithm. The above-mentioned algorithms determine the displacements for each subset center independently and can be considered as a pointwise algorithm. Quite different from these pointwise algorithms, a continuum method (or a global method), in which the surface deformation of the test object throughout the entire image area was represented by the B-spline function, was proposed by Cheng *et al* [109]. In addition, the so-called Q4-DIC developed by Besnard *et al* [110] and the finite element formulation proposed by Sun *et al* [111] can also be categorized into a global method. These techniques ensure the displacement continuity and displacement gradients continuity among calculation points. Thus, they declared that the mismatching of points can be avoided. However, from the

reported results, these two methods seem not to provide higher displacement measurement accuracy than the NR algorithm.

Although various algorithms can be used to achieve sub-pixel displacement, it is worth noting that the most widely used two algorithms in various literature are the iterative spatial domain cross-correlation algorithm and the peak-finding algorithms, due to their simplicity. However, after evaluating their displacement measurement accuracy and precision using computer simulated speckle images with controlled deformation, the iterative spatial domain cross-correlation algorithm with higher accuracy, best stability and broader applicability is highly recommended for practical use [81].

4. Strain field estimation

Now, we can get the full-field displacements to sub-pixel accuracy using the algorithms described above. However, as in many tasks of experimental solid mechanics such as mechanical testing of material and structure stress analysis, full-field strain distributions are more important and desirable. Regrettably, less work has been devoted on the reliable estimation of strain fields. Presumably, this can be attributed to the fact that the displacement gradients (i.e. strains) can be directly calculated using the NR, quasi-NR, LM or genetic algorithm. Alternatively, the strains can be computed as a numerical differentiation process of the estimated displacement.

It should be noted first that the error of estimated displacement gradients using the NR or genetic method normally limits its use only to local strains greater than approximately 0.010 [95]. Besides, although the relationship between the strain and displacement can be described as a numerical differentiation process in mathematical theory, unfortunately, the numerical differentiation is considered as an unstable and risky operation [112, 113], because it can amplify the noise contained in the computed displacement. Therefore, the resultant strains are untrustworthy if they are calculated by directly differentiating the estimated noisy displacements. For example, if the error of displacement estimation is estimated as ± 0.02 pixels and the grid step is 5 pixels, then the error of resultant strain calculated by the forward difference is $\Delta\varepsilon = (|\pm 0.02| + |\pm 0.02|)/5 = 8000\ \mu\varepsilon$, while that calculated by the central difference is $\Delta\varepsilon = (|\pm 0.02| + |\pm 0.02|)/10 = 4000\ \mu\varepsilon$ [78]. An error to that extent will probably hide the underlying strain information of the tested specimen and is unbearable in most cases.

So, it is believed that the accuracy of strain estimation will be improved by smoothing the computed displacement fields first and subsequently differentiating them to calculate strains. Based on these considerations, Sutton *et al* [114] proposed a technique that involves smoothing the computed displacement fields with the penalty finite element method first and subsequently differentiating them to calculate strains. This technique was utilized by Shi *et al* [32] to compute the thermal deformation of electronic packaging. Recently, Meng *et al* [102] further improved the FEM smoothing technique. In addition, the thin plate spline smoothing technique and three other smoothing algorithms were also introduced by Wang *et al* [115] and Tong [116], respectively, to remove the noises contained in displacement fields. Because the noise level contained in the displacement field is significantly decreased after smoothing operation, these techniques substantially increase the precision in resulting strain estimation. However, smoothing noisy discrete data using the penalty finite element method or thin plate spine is quite cumbersome. More recently, to extract the local deformation technique with the PLC band, Xiang *et al* [117] used the moving least-squares (MLS) [118] method to smooth the displacement field followed by a numerical differentiation of the smoothed displacement field to get the strain fields. It is necessary to note that the MLS is a weighted least-squares method for reconstructing continuous functions from a set of unorganized points, and is little different from the following pointwise local least-squares fitting method.

The more practical technique for strain estimation is the pointwise local least-squares fitting technique used and advocated by Wattrisse *et al* [88] and Pan *et al* [78, 101]. In order to analyze the strain localization phenomena that occur during the tension of thin flat steel samples, Wattrisse *et al* [88] implemented a local least-squares method to estimate the strains from the discrete and noisy displacement fields computed by the DIC method. To obtain the strains of the points located at calculation boundaries, a continuity extension of the displacement field is performed at the image boundary. A similar technique was also used by Pan *et al* [101] with a simpler and more effective data processing technique for the calculation of strains for the points located at the image boundary, hole, cracks and the other discontinuity area.

The implementation of the local least-squares fitting technique for strain estimation can be explained as follows. As shown in figure 8, suppose we want to compute the strains of the current point, we first select a square window containing $(2m + 1) \times (2m + 1)$ discrete points (i.e. strain calculation window) around it. If the strain calculation window is small enough, the displacement distributions in it can be approximated as a linear plane; thus, we have

$$\begin{aligned} u(i, j) &= a_0 + a_1 x + a_2 y \\ v(i, j) &= b_0 + b_1 x + b_2 y, \end{aligned} \tag{8}$$

where $i, j = -m$: m are the local coordinates within the strain calculation window, $u(i, j)$ and $v(i, j)$ are the original displacements at location (i, j) obtain by DIC as indicated in figure 8, and $a_{i=0,1,2}, b_{i=0,1,2}$ are the unknown polynomial coefficients to be determined. Equation (8) can be rewritten in matrix form. For the first formulation of equation (8), it can be rewritten as

$$\begin{bmatrix} 1 & -m & -m \\ 1 & -m+1 & -m \\ \vdots & \vdots & \vdots \\ 1 & 0 & 0 \\ \vdots & \vdots & \vdots \\ 1 & m-1 & m \\ 1 & m & m \end{bmatrix} \begin{pmatrix} a_0 \\ a_1 \\ a_2 \end{pmatrix} = \begin{Bmatrix} u(-m, -m) \\ u(-m+1, -m) \\ \vdots \\ u(0, 0) \\ \vdots \\ u(m-1, m) \\ u(m, m) \end{Bmatrix}. \tag{9}$$

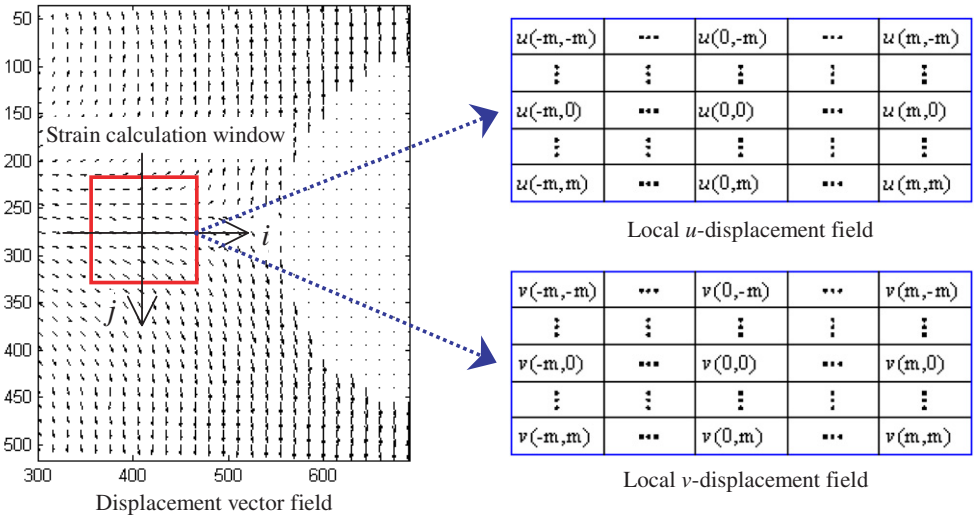

Figure 8. Local strain calculation window containing $(2m + 1) \times (2m + 1)$ discrete displacement data used for strain estimation.

Table 3. Error sources of 2D DIC.

Errors related to specimen, loading and imaging	Speckle pattern Non-parallel between the CCD target and the object surface and out-of-plane displacement Imaging distortion Noises during image acquisition and digitization
Errors related to the correlation algorithm	Subset size Correlation function Sub-pixel algorithm Shape function Interpolation scheme

Thus, the least-squares method can be used to solve the unknown polynomial coefficients. It is important to note that, for the points located at the image boundary or in the vicinity of discontinuity area, the strain calculation window around it may contain less than $(2m + 1) \times (2m + 1)$ points. However, we can still compute strain components using least-squares fitting by simply neglecting these invalid points within the local strain calculation window from equation (9) [102].

Therefore, the desired Cauchy strains or Green strains at the center point of a local sub-region can be computed based on the obtained coefficients $a_{i=0,1,2}$, $b_{i=0,1,2}$. Since the noises can be largely removed in the process of local fitting, thus the accuracy of the calculated strains is greatly improved. However, it is quite important to note that, to obtain reasonable and accurate full-field strain estimation, the following two aspects are important and should be considered. One is the accuracy of displacement fields obtained by DIC, and the other is the size of the local strain calculation window used for fitting. For homogeneous deformation, a large strain calculation window is preferred. However, for inhomogeneous deformation, a proper size of strain calculation window should be selected with care to get a balance between strain, accuracy and smoothness [78, 101, 113, 119]. A small strain calculation window cannot suppress the noise of the displacements, while a large strain calculation window may lead to the unreasonable linear approximation of deformation within the strain calculation window.

5. Displacement measurement error analysis

Compared with other interferometric techniques for deformation measurement, one significant advantage of the 2D DIC is that it has fewer requirements in experimental environment, and can easily be implemented with a simple experimental setup. However, this does not mean that the measurement accuracy of 2D DIC is not or less affected by the measuring system. In contrast, it is noted that the displacement and strain measurement accuracy of 2D DIC relies heavily on the quality of loading system, the perfection of the imaging system and the selection of a particular correlation algorithm. The errors related to various factors are given in table 3. Obviously, estimation of the errors related to different error sources is important to find ways to improve the measurement accuracy of 2D DIC [120]. This section analyzes the possible error sources involved in the implementation of the 2D DIC method. Measures for improving the accuracy and precision of DIC are also recommended.

5.1. Errors related to specimen, loading and imaging

5.1.1. Speckle pattern. The measurement of DIC is closely related to the quality of the speckle pattern on the specimen surface, which may demonstrate distinctly different grayscale distribution characteristics, such as different image contrasts or speckle sizes. Different parameters, such as mean speckle

size [121], subset entropy [122] and sum of square of subset intensity gradients (SSSIG) [123], have been proposed to evaluate the quality of the speckle pattern. Besides, it is important to point out that the speckle pattern quality directly affects the selection of subset size as will be discussed later. For some speckle patterns a large subset must be chosen to provide a reliable result, while for some speckle patterns with sharp contrast, a very small subset containing sufficiently distinctive intensity pattern yields a satisfactory result.

5.1.2. Non-parallel CCD sensor and object surface and out-of-plane displacement. As already mentioned in section 2, the specimen surface must be flat and should be placed parallel to the CCD sensor. This is one of the basic requirements for successful use of the 2D DIC method. Practically, the requirement is approximately rather than perfectly satisfied in an actual experiment because of the existence of non-parallelism between the CCD sensor and object surface before loading and occurrence of out-of-plane displacement during loading.

Theoretical analysis done by Meng *et al* [124] indicates that a non-parallel angle less than 5° introduces a displacement error smaller than 0.01 pixels. In some special cases, for instance, when observing the deformation of a large building or bridge, the optical axis of a camera cannot be placed perpendicular to the specimen surface. A calibration process therefore should be employed to compensate for the errors associated with this off-axis optical setup. Numerical studies conducted by Helm [125] show that the calibration process using a regular grid is able to compensate for off-axis angles as high as 30°. In practice, out-of-plane displacement is unavoidable in actual experiment due to the following factors such as deviation of the specimen surface from an ideal plane, imperfection of a loading device and Poisson's ratio of material [70]. The out-of-plane displacement of the specimen leads to a change in the image-to-object distance. If the camera is placed very close to the test object, the magnification of the recorded images will change dramatically, which yields additional nonuniform in-plane displacements. Two effective methods to alleviate the influence of non-parallelism between the CCD sensor and the object surface and out-of-plane displacement are using a telecentric imaging system or placing the camera far from the specimen to approximate a telecentric imaging system [8, 70].

5.1.3. Image distortions. It is known that a low-cost optical imaging lens somewhat suffers from lens distortion. Recently, the error associated with lens distortion has been recognized and techniques to remove the effect of an imperfect lens have been described. For example, the method proposed by Sutton *et al* [126] incorporates a flat plate with a speckled surface that was displaced in two orthogonal directions over a series of steps to determine a warping function of the imaging system. The same technique was also used to access and remove the lens distortion presented in a high-speed imaging system [69]. Another calibration procedure that incorporates a fine-pitched orthogonal cross-grating plate was used by Zhang *et al* [35]. In this technique, a third-order polynomial warping function was constructed to describe the distortion errors and the coefficients were determined by comparing node locations of the standard cross-grating plate with those in acquired images. More recently, two simple techniques were proposed by Yoneyama [71, 72] for the determination of the radial and tangential distortion amount of a low-cost zoom lens. One technique is implemented by measuring the additional in-plane displacements of the speckle pattern due to lens distortion in rigid body translation, and the other is carried out by analysis of a distorted regular orthogonal grid using the carrier technique with Fourier transform.

For SEM the recorded image may be contaminated by both spatial and drift distortions. Little work has been performed to remove these distortions except the recent experiments performed by Sutton *et al* [45–47]. In their work, spatial distortion removal is performed using a methodology that employs a series of in-plane rigid body motions and a generated warping function. Drift distortion removal is performed using multiple, time-spaced images to extract the time-varying relative displacement field throughout the experiment. Similarly, distortion also presents in AFM or STM images, which results not only from the nonlinear motions of the piezoelectric scanner when responding to the applied voltage but also from its hysteretic and creep effects. Corresponding distortion removal techniques [55, 127] have been developed to alleviate the influence of distortion on displacement measurement using 2D DIC.

5.1.4. Noise. During recording of the specimen surface image, various noises (e.g. shot noise, thermal noise, cut-off noise) are unavoidably presented in the digital images. Recently, Wang *et al* [128] developed a theoretical model to evaluate the influence of noise. It is shown that the random error in the measured displacement (can be quantified by standard deviation error) will proportionally increase with the noise variance. Image noises can be somewhat alleviated through the use of high-performance hardware such as a cooled CCD. In addition, frame averaging during image acquisition is another commonly used effective means to alleviate the influence of image noise. Besides, illumination lighting fluctuation may occur during image capture. However, the influence of illumination lighting fluctuation can be alleviated by using a proper correlation criterion [77]. Particularly, the ZNSSD or ZNCC correlation criterion, which is insensitive to the offset and linear change of illumination lighting, is highly recommended for use.

5.2. Errors related to the correlation algorithm

The algorithm details, such as a correlation criterion, shape function, subset size and sub-pixel interpolation scheme involved in an iterative spatial domain cross-correlation algorithm for an optimization correlation criterion, actually have an effect in the final displacement measurement. The influences of these factors are described as follows. Normally, to better investigate the various correlation algorithms, numerical experiments are utilized to isolate the possible errors caused by the image acquisition system, imperfect loading

and fluctuation of illumination during image capturing, etc. Accordingly, the errors of the computed displacements of the 2D DIC method associated with a correlation algorithm can be decomposed into two components: systematic error or mean bias error (i.e. accuracy) and standard deviation error or random error (i.e. precision) [81].

5.2.1. Subset size. In subset-based DIC, the users must manually select a subset size varying from several pixels to even more than a hundred pixels before the DIC analysis. Since the subset size directly determines the area of the subset being used to track the displacements between the reference and target subsets, it is found to be critical to the accuracy of the measured displacements. To achieve a reliable correlation analysis in DIC, the size of a subset should be large enough so that there is a sufficiently distinctive intensity pattern contained in the subset to distinguish itself from other subsets. On the other hand, however, it is noted that the underlying deformation field of a small subset can readily and accurately be approximated by a first-order or second-order subset shape function, whereas a larger subset size normally leads to larger errors in the approximation of the underlying deformations. For this reason, to guarantee a reliable displacement measurement, a small subset size is preferable in DIC. The above two conflicting demands imply that there is a trade-off between using large and small subset sizes. Recently, by assuming that the adopted shape function can accurately depict the underlying local deformation field and that the gray intensity gradients of image noise are much lower than that of speckle image, a theoretical model has been derived for predicting the displacement measurement precision of DIC and a novel parameter, i.e. SSSIG, has been recommended to select proper subset size for suppressing the influence of noise [123].

5.2.2. Correlation criterion. In actual experimental environment, the digital images are sometimes acquired with significant exposure or lighting variations over the loading history. Tong [77] evaluates the performances of various correlation criteria and the ZNSSD or ZNCC correlation criterion is most robust and reliable for the images with variable lighting or exposure problems. Mathematic derivation also demonstrates that the ZNSSD or ZNCC correlation criterion is insensitive to the offset and linear change of illumination lighting. Thus, the ZNSSD or ZNCC correlation criterion is highly recommended for practical use.

5.2.3. Interpolation scheme. After comparison of bicubic interpolation, B-spline interpolation and biquintic-spline interpolation, a high-order interpolation scheme is highly recommended by Scherier *et al* [80], for reconstruction of the intensity and intensity gradients since it can faithfully represent the intensity, but the computation cost is correspondingly increased. However, a systematic error depending on the sub-pixel displacement of the concerned subset may occur due to the positional intensity interpolation error on sub-pixel reconstruction. It is interesting to note that in the field of fluidics the same phenomenon was observed, and was called the pixel-locking effect [129].

5.2.4. Shape function. It is noted that the underlying deformation field of a small subset can readily and accurately be approximated by a first-order or second-order subset shape function. Systematic errors due to the shape function were investigated by Scherier [74]. Both theoretical and experimental results [75, 130] show that the second-order shape function yields lower systematic error than the linear shape function at approximately the same levels of random error.

As discussed above, the measurements of 2D DIC depend on a number of factors, including both the performance of hardware and correlation algorithm details. It is difficult or impossible to isolate one error source from the others, so the effects of these factors (e.g. speckle pattern, out-of-plane displacement, lens distortion, noise, subset size, sub-pixel registration algorithm, shape function, interpolation scheme) have been investigated separately in previous studies. Currently, there still lacks a substantial theoretical model to predict the accuracy and precision of 2D DIC measurements. We consider that it is still an interesting and challenging problem to quantitatively analyze the accuracy of 2D DIC by considering the influence of each error source. However, based on the previous discussions, the following measures are strongly recommended to be taken for achieving high accuracy in displacement measurement using the 2D DIC method.

(1) Experimental conditions

- increase the contrast of the speckle pattern;
- guarantee parallelism between the CCD target and the test planar specimen surface;
- use a telecentric lens;
- use a high-quality low noise CCD camera and keep stable and even illumination during loading.

(2) Algorithm details

- use a larger subset when the shape function matches the underlying deformation field;
- use the robust and reliable ZNSSD or ZNCC correlation criterion;
- use the improved NR method to optimize the correlation criterion;
- use a high-order shape function;
- use a bicubic spline or biquintic B-spline interpolation scheme.

6. Applications of 2D DIC

Numerous applications of 2D DIC can be found in the literature, which mainly comprises the following three aspects.

(1) 2D DIC can directly be used for quantitatively determining the deformation field and characterizing the deformation mechanism of various materials [88, 117, 131–135] (e.g. metal, composite, polymer, wood, biological materials) subjected to mechanical loading, thermal loading or other loading.

(2) Various mechanical parameters of a material including Young's modulus [10, 35, 48, 50], Poisson's ratio [10, 35, 48, 50], stress intensity factor [136–138], residual stress [38–41] and thermal expansion coefficient [139, 140] can be further identified based on the computed displacement fields or strain fields. A detailed description of identification of the elastic properties of materials using 2D DIC can be found in recent review papers [141, 142].
(3) The computed deformation fields can also be used to validate the FEM [142, 143] or theoretical analysis [38, 49, 52] and to bridge the gap between experiment, simulation and theory.

7. Conclusions

With a history of more than 20 years, DIC has been improved by many researchers and developed into an effective and flexible optical technique for surface deformation measurement from the macroscopic to micro- or even nanoscale. Numerous successful applications in broad fields have already proven it to be a powerful and indispensable tool for deformation measurement and it continues to enjoy a burgeoning popularity. In this review, the 2D DIC technique and its methodologies are systematically reviewed. Emphases are specially placed on the displacement and strain field estimation algorithms. Possible error sources related to different stages of 2D DIC are also discussed and ways to guarantee measurement accuracy are described.

Recall that 2D DIC can only be used for in-plane deformation of a planar object. So, for deformation measurement of a macroscopic object such as structural components, industrial products with a curved surface, the advanced 3D DIC is more practical and effective because it can be used for the 3D profile and deformation measurement of both planar and curved surfaces, and is insensitive to out-of-plane displacement. With the development of a high accuracy stereovision calibration technique, the authors believe that 3D DIC will gain more and more attention and applications than 2D DIC for deformation measurement of macroscopic object. However, for observing and quantitatively measuring microscale deformation at reduced size, the 2D DIC combined with a high-spatial-resolution imaging device (especially, SEM and AFM) will still be the most effective and irreplaceable tool.

References

[1] Rastogi P K 2000 *Photomechanics (Topics in Applied Physics)* (Berlin: Springer)
[2] Sirkis J S and Lim T J 1991 Displacement and strain-measurement with automated grid methods *Exp. Mech.* **31** 382–8
[3] Goldrein H T, Palmer S J P and Huntley J M 1995 Automated fine grid technique for measurement of large-strain deformation maps *Opt. Lasers Eng.* **23** 305–18
[4] Peters W H and Ranson W F 1981 Digital imaging techniques in experimental stress analysis *Opt. Eng.* **21** 427–31
[5] Chu T C *et al* 1985 Applications of digital-image-correlation techniques to experimental mechanics *Exp. Mech.* **25** 232–44
[6] Sutton M A *et al* 1986 Application of an optimized digital correlation method to planar deformation analysis *Image Vis. Comput* **4** 143–50
[7] Peters W H *et al* 1983 Application of digital correlation methods to rigid body mechanics *Opt. Eng.* **22** 738–42
[8] Sutton M A, McNeill S R, Helm J D and Chao Y J 2000 Advances in two-dimensional and three-dimensional computer vision *Topics in Applied Physics* vol 77 ed P K Rastogi (Berlin: Springer) pp 323–72
[9] Schreier H W 2003 Investigation of two and three-dimensional image correlation techniques with applications in experimental mechanics *PhD Thesis* University of South Carolina
[10] Zhang D, Zhang X and Cheng G 1999 Compression strain measurement by digital speckle correction *Exp. Mech.* **39** 62–5
[11] Zhou P and Goodson K E 2001 Subpixel displacement and deformation gradient measurement using digital image/speckle correlation *Opt. Eng.* **40** 1613–20
[12] Bay B K 1995 Texture correlation—a method for the measurement of detailed strain distributions within trabecular bone *J. Orthop. Res* **13** 258–67
[13] Chen D J, Chiang F P, Tan Y S and Don H S 1993 Digital speckle-displacement measurement using a complex spectrum method *Appl. Opt.* **32** 1839–49
[14] Gaudette G R, Todaro J, Krukenkamp I B and Chiang F P 2001 Computer aided speckle interferometry: a technique for measuring deformation of the surface of the heart *Ann. Biomed. Eng.* **29** 775–80
[15] Sjodahl M and Benckert L R 1993 Electronic speckle photography: analysis of an algorithm giving the displacement with subpixel accuracy *Appl. Opt.* **32** 2278–84
[16] Sjodahl M and Benckert L R 1994 Systematic and random errors in electronics speckle photography *Appl. Opt.* **33** 7461–71
[17] Sjodahl M 1994 Electronic speckle photography—increased accuracy by nonintegral pixel shifting *Appl. Opt.* **33** 6667–73
[18] Sjodahl M 1997 Accuracy in electronic speckle photography *Appl. Opt.* **36** 2875–85
[19] Willert C E and Gharib M 1991 Digital particle image velocimetry *Exp. Fluids* **10** 181–93
[20] Scarano F 2002 Iterative image deformation methods in PIV *Meas. Sci. Technol.* **13** R1–19
[21] Adrian R J 2005 Twenty years of particle image velocimetry *Exp. Fluids* **39** 159–69
[22] White D J, Take W A and Bolton M D 2003 Soil deformation measurement using particle image velocimetry (PIV) and photogrammetry *Geotechnique* **53** 619–31
[23] Lee S G *et al* 2008 Large strain deformation field in machining *Metall. Mater. Trans.* **37A** 1633–43
[24] Luo P F *et al* 1993 Accurate measurement of three-dimensional displacement in deformable bodies using computer vision *Exp. Mech.* **33** 123–32
[25] Helm J D, McNeil S R and Sutton M A 1996 Improved three-dimensional image correlation for surface displacement measurement *Opt. Eng.* **35** 1911–20
[26] Garcia D, Orteu J J and Penazzi L 2002 A combined temporal tracking and stereo-correlation technique for accurate measurement of 3D displacements: application to sheet metal forming *J. Mater. Process. Technol.* **125** 736–42
[27] Pan B, Xie H M, Yang L H and Wang Z Y 2009 Accurate measurement of satellite antenna surface using three-dimensional digital image correlation technique *Strain* **45** 194–200
[28] Bay B K *et al* 1999 Digital volume correlation: three-dimensional strain mapping using x-ray tomography *Exp. Mech.* **39** 217–26

[29] Smith T S, Bay B K and Rashid M M 2002 Digital volume correlation including rotational degrees of freedom during minimization *Exp. Mech* **42** 272–8

[30] Yamaguch I 1981 Speckle displacement and deformation in the diffraction and image fields for small object deformation *Opt. Acta* **28** 1359–76

[31] Brillaud J and Lagattu F 2002 Limits and possibilities of laser speckle and white-light image-correlation methods: theory and experiments *Appl. Opt.* **41** 6603–13

[32] Shi X Q *et al* 2004 *In-situ* micro-digital image speckle correlation technique for characterization of materials' properties and verification of numerical models *IEEE Trans. Compon. Packag. Technol.* **27** 659–67

[33] Sun Z L, Lyons J S and McNeill S R 1997 Measuring microscopic deformations with digital image correlation *Opt. Lasers Eng.* **27** 409–28

[34] Pitter M C *et al* 2002 Focus errors and their correction in microscopic deformation analysis using correlation *Opt. Eng.* **23** 1361–7

[35] Zhang D S, Luo M and Arola D D 2006 Displacement/strain measurements using an optical microscope and digital image correlation *Opt. Eng.* **45** 033605

[36] Berfield T A, Patel H K, Shimmin R G, Braun P V, Lambros J and Sottos N R 2006 Fluorescent image correlation for nanoscale deformation measurements *Small* **2** 631–5

[37] Franck C *et al* 2007 Three-dimensional full-field measurements of large deformations in soft materials using confocal microscopy and digital volume correlation *Exp. Mech.* **47** 427–38

[38] Sabate N *et al* 2006 Measurement of residual stresses in micromachined structures in a microregion *Appl. Phys. Lett.* **88** 071910

[39] Keller J *et al* 2006 FibDAC—residual stress determination by combination of focused ion beam technique and digital image correlation *Mater. Sci. Forum* **524–525** 121–6

[40] Sabate N *et al* 2006 Digital image correlation of nanoscale deformation fields for local stress measurement in thin films *Nanotechnology* **17** 5264–70

[41] Sabate N *et al* 2007 Residual stress measurement on a MEMS structure with high-spatial resolution *J. Microelectromech. Syst.* **16** 365–72

[42] Kang J *et al* 2005 Microscopic strain mapping using scanning electron microscopy topography image correlation at large strain *J. Strain Anal. Eng. Des.* **40** 559–70

[43] Wang H *et al* 2006 Error analysis of digital speckle correlation method under scanning electron microscope *Exp. Tech.* **30** 42–5

[44] Lagattu F *et al* 2006 In-plane strain measurements on a microscopic scale by coupling digital image correlation and an *in situ* SEM technique *Mater. Charact.* **56** 10–8

[45] Sutton M A *et al* 2006 Metrology in a scanning electron microscope: theoretical developments and experimental validation *Meas. Sci. Technol.* **17** 2613–22

[46] Sutton M A *et al* 2007 Scanning electron microscopy for quantitative small and large deformation measurements: Part I. SEM imaging at magnifications from 200 to 10,000 *Exp. Mech.* **47** 775–87

[47] Sutton M A *et al* 2007 Scanning electron microscopy for quantitative small and large deformation measurements: Part II. Experimental validation for magnifications from 200 to 10,000 *Exp. Mech.* **47** 789–804

[48] Chasiotis I and Knauss W G 2002 A new microtensile tester for the study of MEMS materials with the aid of atomic force microscopy *Exp. Mech.* **42** 51–7

[49] Knauss W G, Chasiotis I and Huang Y 2003 Mechanical measurements at the micron and nanometer scales *Mech. Mater.* **35** 217–31

[50] Cho S W *et al* 2005 Young's modulus, Poisson's ratio and failure properties of tetrahedral amorphous diamond-like carbon for MEMS devices *J. Micromech. Microeng.* **15** 728–35

[51] Chasiotis I and Knauss W G 2002 Size effects determined from tensile tests of perforated MEMS scale specimens *Proc. MRS 687 (Boston, MA)* pp 241–6

[52] Cho S W, Cardenas-Garcia J F and Chasiotis I 2005 Measurement of nanodisplacements and elastic properties of MEMS via the microscopic hole method *Sensors Actuators* A **120** 163–71

[53] Chasiotis I 2004 Mechanics *IEEE Trans. Device Mater. Reliab.* **4** 176–88

[54] Chang S *et al* 2005 Nanoscale in-plane displacement evaluation by AFM scanning and digital image correlation processing *Nanotechnology* **16** 344–9

[55] Sun Y F and Pang J H L 2006 AFM image reconstruction for deformation measurements by digital image correlation *Nanotechnology* **17** 933–9

[56] Li X D *et al* 2007 *In situ* nanoscale in-plane deformation studies of ultrathin polymeric films during tensile deformation using atomic force microscopy and digital image correlation techniques *IEEE Trans. Nanotechnology* **6** 4–12

[57] Li X D *et al* 2006 Nanoscale deformation and cracking studies of advanced metal evaporated magnetic tapes using atomic force microscopy and digital image correlation techniques *Meas. Sci. Technol.* **22** 835–44

[58] Sun Y F, Pang J H L and Fan W 2007 Nanoscale deformation measurement of microscale interconnection assemblies by a digital image correlation technique *Nanotechnology* **18** 395504

[59] Vendroux G and Knauss WG 1998 Submicron deformation field measurements: Part 1. Developing a digital scanning tunneling microscope *Exp. Mech.* **38** 18–23

[60] Vendroux G and Knauss W G 1998 Submicron deformation field measurements: Part 2. Improved digital image correlation *Exp. Mech.* **38** 86–92

[61] Vendroux G, Schmidt N and Knauss W G 1998 Submicron deformation field measurements: Part 3. Demonstration of deformation determinations *Exp. Mech.* **38** 154–60

[62] Kawahashi M and Hirahara H 2000 Velocity and density field measurements by digital speckle method *Opt. Laser Technol.* **32** 575–82

[63] Barthelat F *et al* 2003 Dynamic torsion testing of nanocrystalline coatings using high-speed photography and digital image correlation *Exp. Mech.* **43** 331–40

[64] Tong W *et al* 2005 Time-resolved strain mapping measurements of individual Portevin–Le Chatelier deformation bands *Scr. Mater.* **53** 87–92

[65] Yang F J, He X Y and Quan C G 2006 Characterization of dynamic microgyroscopes by use of temporal digital image correlation *Appl. Opt.* **45** 7785–90

[66] Luo H, Lu H and Leventis N 2006 The compressive behavior of isocyanate-crosslinked silica aerogel at high strain rates *Mech. Time-Dependent Mater.* **10** 83–111

[67] Kirugulige M S, Tippur H V and Denney T S 2007 Measurement of transient deformations using digital image correlation method and high-speed photography: application to dynamic fracture *Appl. Opt.* **46** 5083–96

[68] Siebert T *et al* 2007 High-speed digital image correlation: error estimations and applications *Opt. Eng.* **46** 051004

[69] Tiwari V, Sutton M A and McNeill S R 2007 Assessment of high speed imaging systems for 2D and 3D deformation measurements: methodology development and validation *Exp. Mech.* **47** 561–79

[70] Sutton M A, Yan J H, Tiwari V, Schreier W H and Orteu J J 2008 The effect of out-of-plane motion on 2D and 3D digital image correlation measurements *Opt. Lasers Eng.* **46** 746–57

[71] Yoneyama S, Kikuta H, Kitagawa A and Kitamura K 2006 Lens distortion correction for digital image correlation by measuring rigid body displacement *Opt. Eng.* **45** 023602

[72] Yoneyama S, Kitagawa A, Kitamura K and Kikuta H 2006 In-plane displacement measurement using digital image correlation with lens distortion correction *JSME Int. J.* A **49** 458–67

[73] Pan B and Xie H M 2009 Assessment and correction of lens distortion for digital image correlation *Acta Metro. Sin.* **30** 62–7 (in Chinese)

[74] Schreier H W and Sutton M A 2002 Systematic errors in digital image correlation due to undermatched subset shape functions *Exp. Mech.* **42** 303–10

[75] Lu H and Cary P D 2000 Deformation measurement by digital image correlation: implementation of a second-order displacement gradient *Exp. Mech.* **40** 393–400

[76] Giachetti A 2000 Matching techniques to compute image motion *Image Vis. Comput.* **18** 247–60

[77] Tong W 2005 An evaluation of digital image correlation criteria for strain mapping applications *Strain* **41** 167–75

[78] Pan B, Xie H M, Guo Z Q and Hua T 2007 Full-field strain measurement using a two-dimensional Savitzky–Golay digital differentiator in digital image correlation *Opt. Eng.* **46** 033601

[79] Press William H 2003 *C*++ *Numerical Algorithms* (Beijing: Publishing House of Electronics Industry)

[80] Schreier H W, Braasch J R and Sutton M A 1999 Systematic errors in digital image correlation caused by intensity interpolation *Opt. Eng.* **39** 2915–21

[81] Pan B *et al* 2006 Performance of sub-pixel registration algorithms in digital image correlation *Meas. Sci. Technol.* **17** 1615–21

[82] Zhang Z F *et al* 2006 A novel coarse-fine search scheme for digital image correlation method *Measurement* **39** 710–8

[83] Hild F *et al* 2002 Multiscale displacement field measurements of compressed mineral-wool samples by digital image correlation *Appl. Opt.* **41** 6815–28

[84] Pan B, Xie H, Xia Y and Wang Q 2009 Large deformation measurement based on reliable initial guess in digital image correlation method *Acta Optica Sin.* **29** 400–6 (in Chinese)

[85] Pan B and Xie H M 2007 Digital image correlation method with differential evolution *J. Optoelectron. Laser* **18** 100–3 (in Chinese)

[86] Pan B 2009 Reliability-guided digital image correlation for image deformation measurement *Appl. Opt.* **48** 1535–42

[87] Hung P C and Voloshin P S 2003 In-plane strain measurement by digital image correlation *J. Braz. Soc. Mech. Sci. Eng.* **25** 215–21

[88] Wattrisse B C, Muracciole A and Nemoz-Gaillard J M 2001 Analysis of strain localization during tensile tests by digital image correlation *Exp. Mech.* **41** 29–39

[89] Pan B, Xu B Q, Chen D and Feng J 2005 Sub-pixel registration using quadratic surface fitting in digital image correlation *Acta Metro. Sin.* **26** 128–34 (in Chinese)

[90] Wang M *et al* 2008 A weighting window applied to the digital image correlation method *Opt. Laser Technol.* **41** 154–8

[91] Hua T *et al* 2007 A new micro-tensile system for measuring the mechanical properties of low dimensional materials—fibers and films *Polym. Test* **26** 513–8

[92] Sun W, Quan C G, Tay C J and He X Y 2007 Global and local coordinates in digital image correlation *Appl. Opt.* **46** 1050–6

[93] Sun W, Quan C G and He X Y 2008 Dynamic characterization of a microgyroscope by digital image spectrum correlation *Opt. Eng.* **47** 3

[94] Wim V P, Assen A S, Ilia R R, Stijn D P, Joris D and Ventseslav C S 2008 Study of the deformation characteristics of window security film by digital image correlation techniques *Opt. Lasers Eng.* **46** 390–7

[95] Bruck H A, McNeil S R, Sutton M A and Peters W H 1989 Digital image correlation using Newton–Raphson method of partial differential correction *Exp. Mech.* **29** 261–7

[96] Wang H W and Kang Y L 2001 Improved digital speckle correlation method and its application in fracture analysis of metallic foil *Opt. Eng.* **41** 2793–8

[97] Davis C Q and Dennis M F 1998 Statistics of subpixel registration algorithms based on spatiotemporal gradients or block matching *Opt. Eng.* **37** 1290–8

[98] Zhang J and Jin G C 2003 Application of an improved subpixel registration algorithm on digital speckle correlation measurement *Opt. Laser Technol.* **35** 533–42

[99] Pan B, Xu B Q and Li K J 2005 Performance of gradient operators in algorithm of gradient-based sub-pixel registration *Opt. Technol.* **31** 26–31 (in Chinese)

[100] Pan B, Chen P and Xu B Q 2005 In-plane displacements measurement by gradient-based digital image correlation *Proc. SPIE* **5852** 544–51

[101] Pan B, Asundi A, Xie H M and Gao J X 2009 Digital image correlation using iterative least squares and pointwise least squares for displacement field and strain field measurements *Opt. Lasers Eng.* at press

[102] Meng L B, Jin G C and Yao X F 2007 Application of iteration and finite element smoothing technique for displacement and strain measurement of digital speckle correlation *Opt. Lasers Eng.* **45** 57–63

[103] Pilch A, Mahajan A and Chu T C 2004 Measurement of whole-field surface displacements and strain using a genetic algorithm based intelligent image correlation method *Trans. ASME, J. Dyn. Syst. Meas. Control* **126** 479–88

[104] Ma S P and Jin G C 2003 Digital speckle correlation method improved by genetic algorithm *Acta Mech. Solida Sin.* **16** 366–73

[105] Jin H Q and Bruck H A 2005 Pointwise digital image correlation using genetic algorithms *Exp. Tech.* **29** 36–9

[106] Jin H Q and Bruck H A 2005 Theoretical development for pointwise digital image correlation *Opt. Eng.* **44** 1–14

[107] Hwang S F, Horn J T and Wang H J 2008 Strain measurement of SU-8 photoresist by a digital image correlation method with a hybrid genetic algorithm *Opt. Lasers Eng.* **46** 281–9

[108] Pitter M C, See C W and Somekh M G 2001 Subpixel microscopic deformation analysis using correlation and artificial neural networks *Opt Exp.* **8** 322–7

[109] Cheng P *et al* 2002 Full-field speckle pattern image correlation with B-spline deformation function *Exp. Mech.* **42** 344–52

[110] Besnard G *et al* 2006 Finite-element displacement fields analysis from digital images: application to portevin-le chatelier bands *Exp. Mech.* **46** 789–803

[111] Sun Y F *et al* 2005 Finite element formulation for a digital image correlation method *Appl. Opt.* **44** 7357–63

[112] Luo J W, Ying K, He P and Bai J 2005 Properties of Savitzky–Golay digital differentiators *Digit. Signal Process.* **15** 122–36

[113] Luo J W, Bai J, He P and Ying K 2004 Axial strain calculation using a low-pass digital differentiator in ultrasound elastography *IEEE Trans. Ultrason. Ferroelectr. Freq. Control* **51** 1119–27

[114] Sutton M A, Turner J L, Bruck H A and Chao T A 1991 Full-field representation of discretely sampled surface deformation for displacement and strain analysis *Exp. Mech.* **31** 168–77

[115] Wang C C B *et al* 2002 An automated approach for direct measurement of two-dimensional strain distributions

within articular cartilage under unconfined compression *Trans. ASME, J. Biomech. Eng.* **124** 557–67
[116] Tong W 1997 Detection of plastic deformation patterns in a binary aluminum alloy *Exp. Mech.* **37** 452–9
[117] Xiang G F *et al* 2007 Time-resolved deformation measurements of the Portevin–Le Chatelier bands *Scr. Mater.* **56** 721–4
[118] Lancaster P and Salkauskas K 1981 Surfaces generated by moving least-squares methods *Math. Comput.* **37** 141–58
[119] Pan B *et al* 2006 Data smoothing and strain estimation using Savitzky-Golay filters in digital image correlation *Key Eng. Mater.* **326–328** 155–8
[120] Haddadi H and Belhabib S 2008 Use of rigid-body motion for the investigation and estimation of the measurement errors related to digital image correlation technique *Opt. Lasers Eng.* **46** 185–96
[121] Lecompte D *et al* 2006 Quality assessment of speckle patterns for digital image correlation *Opt. Lasers Eng.* **44** 1132–45
[122] Yaofeng S and Pang J H L 2007 Study of optimal subset size in digital image correlation of speckle pattern images *Opt. Lasers Eng.* **45** 967–74
[123] Pan B, Xie H M, Wang Z Y, Qian K M and Wang Z Y 2008 Study on subset size selection in digital image correlation for speckle patterns *Opt. Express* **16** 7037–48
[124] Meng L B, Jin G C and Yao X F 2006 Errors caused by misalignment of the optical camera axis and the object surface in the DSCM *J. Tsinghua Univ. (Sci. Technol.)* **46** 1930–2
[125] Helm J D and Deanner J R 2004 Off-axis two-dimensional digital image correlation *Proc. 2004 SEM X Int. Congress & Exposition on Experimental and Applied Mechanics (Costa Mesa)* 2004-06-1-10CT: SEM
[126] Schreier H W, Garcia D and Sutton M A 2004 Advances in light microscope stereo vision *Exp. Mech.* **44** 278–88
[127] Jin H and Bruck H A 2005 A new method for characterizing nonlinearity in scanning probe microscopes using digital image correlation *Nanotechnology* **16** 1849–55
[128] Wang Z Y *et al* 2007 Statistical analysis of the effect of intensity pattern noise on the displacement measurement precision of digital image correlation using self-correlated images *Exp. Mech.* **47** 701–7
[129] Huang H, Dabiri D and Gharib M 1997 On errors of digital particle image velocimetry *Meas. Sci. Technol.* **8** 1427–40
[130] Pan B, Xie H M, Gao J X and Asundi A 2008 Improved speckle projection profilometry for out-of-plane shape measurement *Appl. Opt.* **47** 5527–33
[131] Bastawros A F, Bart-Smith H and Evans A G 2000 Experimental analysis of deformation mechanisms in a closed-cell aluminum alloy foam *J. Mech. Phys. Solids* **48** 301–22
[132] Chevalier L *et al* 2001 Digital image correlation used to analyze the multiaxial behavior of rubber-like materials *Eur. J. Mech.* A **20** 169–87
[133] Abanto-Bueno J and Lambros J 2002 Investigation of crack growth in functionally graded materials using digital image correlation *Eng. Fract. Mech.* **69** 1695–711
[134] Perie J N *et al* 2002 Analysis of a multiaxial test on a C/C composite by using digital image correlation and a damage model *Exp. Mech.* **42** 318–28
[135] Chiang F P 2008 Micro-/nano-speckle method with applications to materials, tissue engineering and heart mechanics *Strain* **44** 27–39
[136] Mcneill S R, Peters W H and Sutton M A 1987 Estimation of stress intensity factor by digital image correlation *Eng. Fract. Mech.* **28** 101–12
[137] Roux S and Hild F 2006 Stress intensity factor measurements from digital image correlation: post-processing and integrated approaches *Int. J. Fract* **140** 141–57
[138] Yoneyama S, Morimoto Y and Takashi M 2006 Automatic evaluation of mixed-mode stress intensity factors utilizing digital image correlation *Strain* **42** 21–9
[139] Lyons J S, Liu J and Sutton M A 1996 High-temperature deformation measurement using digital image correlation *Exp. Mech* **36** 64–70
[140] Pan B, Xie H M, Hua T and Asundi A 2009 Measurement of coefficient of thermal expansion of films using digital image correlation method *Polym. Test.* **28** 75–83
[141] Hild F and Roux S 2006 Digital image correlation: from displacement measurement to identification of elastic properties—a review *Strain* **42** 69–80
[142] Avril S *et al* 2008 Overview of identification methods of mechanical parameters based on full-field measurements *Exp. Mech.* **48** 381–402
[143] Sun Y F and Pang J H L 2008 Experimental and numerical investigations of near-crack-tip deformation in a solder alloy *Acta Mater.* **56** 537–48